Supplementary Information

Dynamic Rigidity Changes Enable Rapid Cell Migration on Soft Substrates

Jiapeng Yang[#, 1, 2, 3], Yu Zhang[#, 1, 2], Shuo Wang[#, 4], Peng Wang[3], Liang Dong[2], Luofei Li[2], Yuanqi Cheng[2], Xiaoyu Huang[2], Bin Xue[2], Wei Wang[2], Chunping Jiang[, 1, 4], Xiaosong Gu[1, 4, 6], Qiang Wei[*, 3] and Yi Cao[*, 1, 2, 5, 7]*

[1] Jinan Microecological Biomedicine Shandong Laboratory, Jinan, 250118, China

[2] National Laboratory of Solid State Microstructures, Department of Physics, Nanjing University, Nanjing, 210093, China.

[3] College of Polymer Science and Engineering, State Key Laboratory of Polymer Materials and Engineering, Sichuan University, Chengdu, 610065, China.

[4] Division of Hepatobiliary and Transplantation Surgery, Department of General Surgery Nanjing Drum Tower Hospital, the Affiliated Hospital of Medical School, Nanjing University, Nanjing, 210008, China.

[5] Wenzhou Institute, University of Chinese Academy of Sciences, Wenzhou, 325001, China.

[6] Key Laboratory of Neuroregeneration of Jiangsu and Ministry of Education, NMPA Key Laboratory for Research and Evaluation of Tissue Engineering Technology Products, Nantong University, Nantong, 226001, China.

[7] Chemistry and Biomedicine Innovation Center (ChemBIC), MOE Key Laboratory of High Performance Polymer Materials and Technology, School of Chemistry and Chemical Engineering, Nanjing University; Nanjing, 210023, China.

[#] These authors contributed equally.

[*] Correspondence: caoyi@nju.edu.cn; wei@scu.edu.cn; chunpingjiang@nju.edu.cn.

Supplementary Movie Files

Supplementary Movie 1 HMSCs on soft substrates with a Young’s modulus of approximately 1.6 kPa. hMSCs exhibit minimal migration on soft substrates with a Young’s modulus of ~1.6 kPa.

Supplementary Movie 2 HMSCs on rigid substrates with a Young’s modulus of approximately 13.0 kPa. hMSCs migrate efficiently on rigid substrates with a Young’s modulus of ~13.0 kPa.

Supplementary Movie 3 HMSCs on PYP hydrogels with fast cyclic rigidity changes (1 min on/off). hMSCs exhibit rapid migration under cyclic rigidity changes with 1-min cycles.

Supplementary Movie 4 HMSCs on PYP hydrogels with cyclic rigidity changes (5 min on/off). hMSCs migrate rapidly under cyclic rigidity changes with 5-min cycles.

Supplementary Movie 5 HMSCs on PYP hydrogels with slow cyclic rigidity changes (10-min on/off). No significant changes in migration are observed under cyclic rigidity changes with 10-min cycles.

Supplementary Movie 6 HMSCs on soft substrates with a Young’s modulus of approximately 2.2 kPa. hMSCs exhibit minimal migration on soft substrates with a Young’s modulus of ~2.2 kPa.

Supplementary Movie 7 HMSCs on polyacrylamide hydrogels (PA gels, Young's modulus ~2.2 kPa). Cyclic illumination has no impact on cell migration on photo-insensitive PA gels.

Supplementary Movie 8 HMSCs on PYP hydrogels with fast cyclic rigidity changes for the first 6 hours, followed by static rigidity in the final 6 hours. Cell migration slows down after the cessation of fast cyclic rigidity changes.

Supplementary Movie 9 HMSCs on PYP hydrogels with fast cyclic rigidity changes, supplemented with a Rac1 inhibitor. The inhibition of Rac1 results in a significant reduction in cell migration on dynamically changing substrates.

Supplementary Movie 10 HMSCs on PYP hydrogels with fast cyclic rigidity changes, supplemented with latrunculin A. The inhibition of actin polymerization by latrunculin A leads to a marked reduction in cell migration on dynamic substrates.

Supplementary Movie 11 HMSCs on PYP hydrogels with fast cyclic rigidity changes, supplemented with β1-integrin blocking. The blockade of β1-integrin results in a significant reduction in cell migration on dynamic substrates.

Supplementary Movie 12 Actin retrograde flow dynamics of hMSCs on PYP hydrogels with fast cyclic rigidity changes (1 min on/off).

Supplementary Movie 13 Actin retrograde flow dynamics of hMSCs on rigid substrates with a Young's modulus of approximately 13.0 kPa.

Supplementary Movie 14 Actin retrograde flow dynamics of hMSCs on soft substrates with a Young's modulus of approximately 2.2 kPa and 1.6 kPa.

Supplementary Movie 15 Focal adhesion dynamics of hMSCs on PYP hydrogels with fast cyclic rigidity changes (1 min on/off).

Supplementary Movie 16 Focal adhesion dynamics of hMSCs on rigid substrates with a Young's modulus of approximately 13.0 kPa.

Supplementary Movie 17 Focal adhesion dynamics of hMSCs on rigid substrates with a Young's modulus of approximately 2.2 kPa.

Supplementary Movie 18 Focal adhesion dynamics of hMSCs on rigid substrates with a Young's modulus of approximately 1.6 kPa.

Supplementary Movie 19 HMSCs overexpressing Talin on PYP hydrogels with fast cyclic rigidity changes. hMSCs overexpressing Talin shift to a mesenchymal migration mode on dynamic soft substrates.

Supplementary Movie 20 HMSCs on PYP hydrogels with fast cyclic rigidity changes, supplemented with non-phototoxic Blebbistatin inhibitors. Inhibition of myosin II activity with Blebbistatin significantly reduces cell migration on dynamic substrates.

Supplementary Movie 21 HMSCs on PYP hydrogels with fast cyclic rigidity changes, with a larger softening amplitude from the rigid state. Cells exhibit faster migration speed, shorter elongation duration, and higher snap-back frequency during migration.

Table S1. Model parameters.

Parameter	Meaning	Value	Ref
n_c	Initial number of integrin	75	David J. Odde, Science, 2008[1]
r_{on}^0	Binding rate	$1\ s^{-1}$	David J. Odde, Science, 2008[1]
r_{off}^0	Zero force dissociation rate	$0.1\ s^{-1}$	David J. Odde, Science, 2008[1]
F_{cr}	Threshold reinforcement force	$3\ pN$	Gong, Z, PNAS, 2018[2]
α	Integrin density increment rate	$0.2\ pN^{-1}$	Gong, Z, PNAS, 2018[2]
F_b	Characteristic breakage force	$2\ pN$	David J. Odde, Science, 2008[1]
V_r	Retrograde flow velocity	$120\ nm \cdot s^{-1}$	David J. Odde, Science, 2008[1]
k_c	Stiffness of clutch	$5\ pN \cdot nm^{-1}$	David J. Odde, Science, 2008[1]
k_s	Stiffness of ECM	$1.6\sim2.2\ kPa$	This work (main independent variable).
R_0	Cell radius before spreading (Just for calculating f_r)	$5\ \mu m$	Gong, Z, PNAS, 2018[2]
R_i	Initial cell radius	$20\ \mu m$	Gong, Z, PNAS, 2018[2]
k_m	Effective stiffness of cytoskeleton	$0.1\ pN \cdot nm^{-1}$	Gong, Z, PNAS, 2018[2]
η_m	Effective viscosity of cytoskeleton	$100\ pN \cdot s \cdot nm^{-1}$	Gong, Z, PNAS, 2018[2]
h	Thickness of lamellipodium	$200\ nm$	Gong, Z, PNAS, 2018[2]
V_p	Polymerization speed	$127\ nm \cdot s^{-1}$	Based on Gong, Z, PNAS, 2018[2]
k_e	Engage speed of integrin	$3.75\ \cdot 10^{-6}\ ms^{-1}$	Based on Cheng, B, Sci Adv, 2020[3]

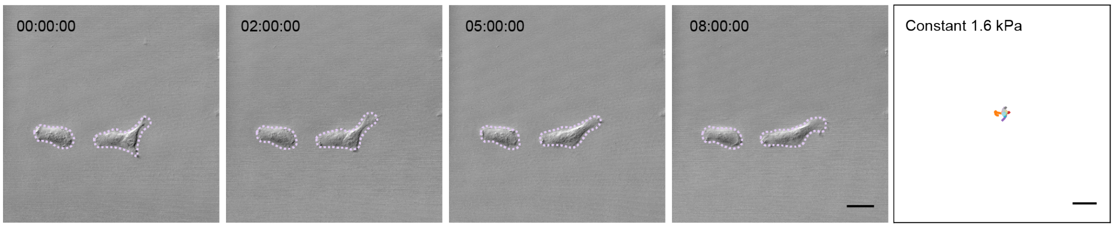

Figure S1 Time series of images of hMSCs on static soft PYP hydrogel (Young's modulus of ~1.6 kPa). The far-right panel shows the trajectories of ~20 randomly selected migrating cells under the condition over 12 hours. Times are indicated in hour:minute:second. Scale bar is 50 µm for all panels.

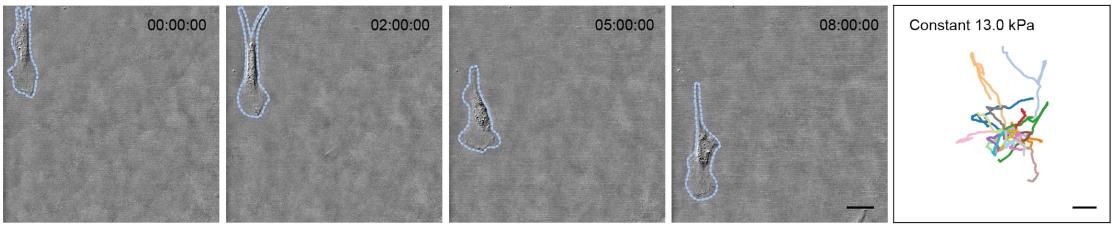

Figure S2 Time series of images of hMSCs on static rigid PYP hydrogel (Young's modulus of ~13.0 kPa). The far-right panel shows the trajectories of ~20 randomly selected migrating cells under the condition over 12 hours. Times are indicated in hour:minute:second. Scale bar is 50 µm for all panels.

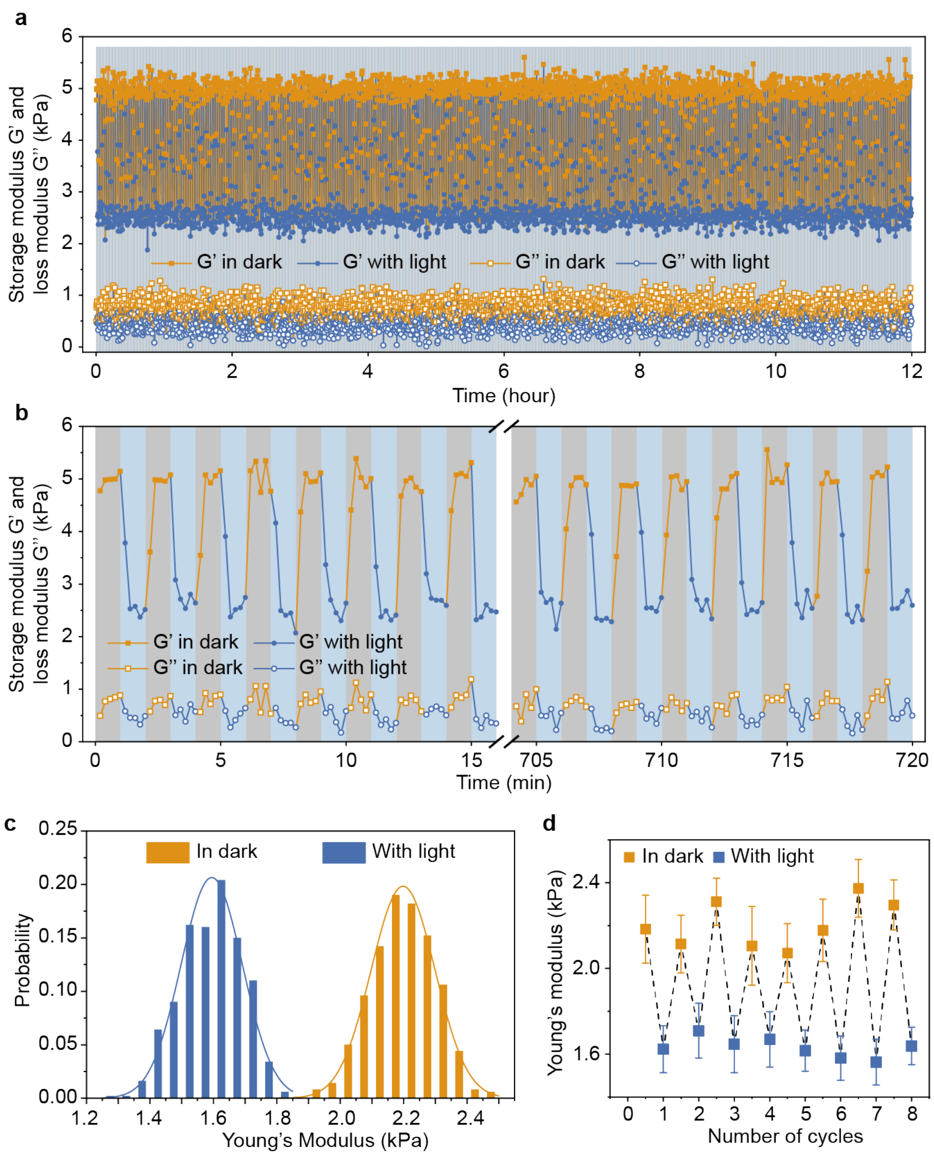

Figure S3 (a-b) Rheological characterization of the storage modulus (G') and loss modulus (G'') of the PYP hydrogel under cyclical switching between dark and light conditions (1 min on/off). The complete dataset (a) from the 12-hour experiment, demonstrating the stability and reversibility of the hydrogel's mechanical response. Zoomed-in views (b) highlighting the detailed, synchronized modulation of G' and G'' during representative intervals at the beginning and end of the test period. (c) Young's modulus distributions of the PYP hydrogel under dark conditions and with light illumination. The curves correspond to fittings by Gaussion distribution. n=500 force-deformation traces were collected for each set of data. The approaching curves were fitted to the Hertz model to obtain the Young's modulus of each indentation point.
(d) AFM nanoindentation characterization of the Young's moduli of the PYP hydrogels in response to cyclic blue light illumination (1 min on/off). n=20 force-deformation traces were collected for each set of data. The approaching curves were fitted to the Hertz model to obtain the Young's modulus of each indentation point. Data are presented as mean values +/- standard deviation.

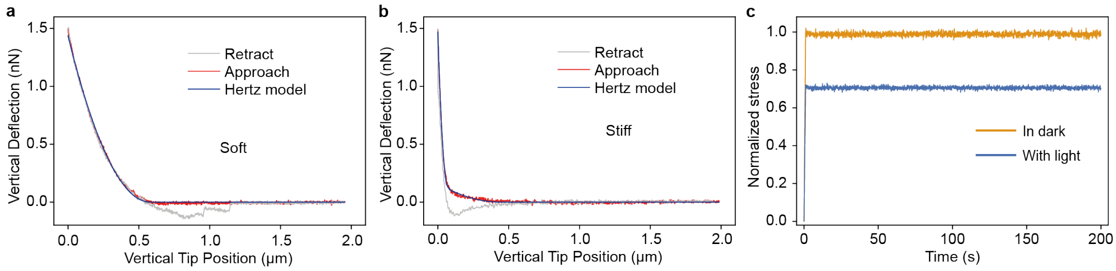

Figure S4 (a-b) Representative AFM force vs. extension traces for soft (a) and rigid (b) hydrogels and fittings by the Hertz model. (c) Stress relaxation curves of the PYP hydrogel under dark conditions and with light illumination by rheological characterization.

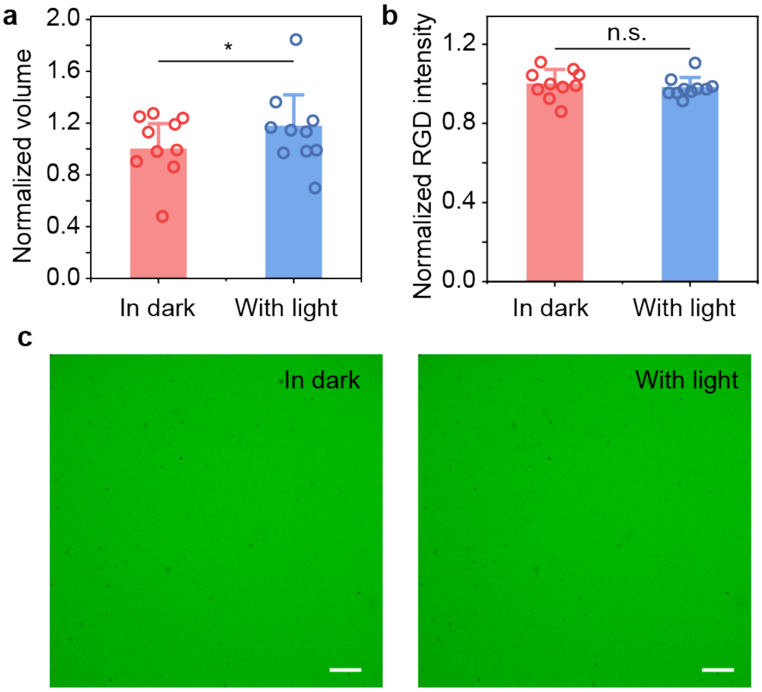

Figure S5 (a) Normalized volume comparison of PYP hydrogel under dark conditions and with light illumination. In a, each from 10 independent experiments, * represents p < 0.1. p = 0.092, unpaired, two-tailed t-test; in b, n.s. represents p > 0.1, p = 0.52, unpaired, two-tailed t-test. Data are presented as mean values +/- standard deviation. (b-c) Normalized RGD intensity comparison of PYP hydrogel under dark conditions and with light illumination. Scale bar is 50 μm for all panels. In b, each from 10 independent experiments. Data are presented as mean values +/- standard deviation.

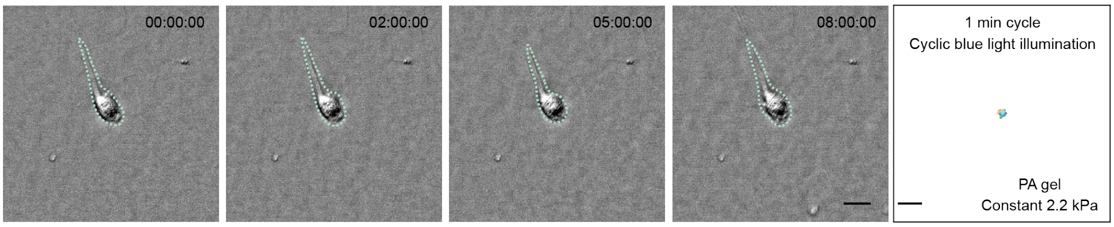

Figure S6 Time series of images of hMSCs on photo-insensitive polyacrylamide hydrogels (PA gel, Young's modulus of ~2.2 kPa). The far-right panel shows the trajectories of ~20 randomly selected migrating cells under the condition over 12 hours. Times are indicated in hour:minute:second. Scale bar is 50 μm for all panels.

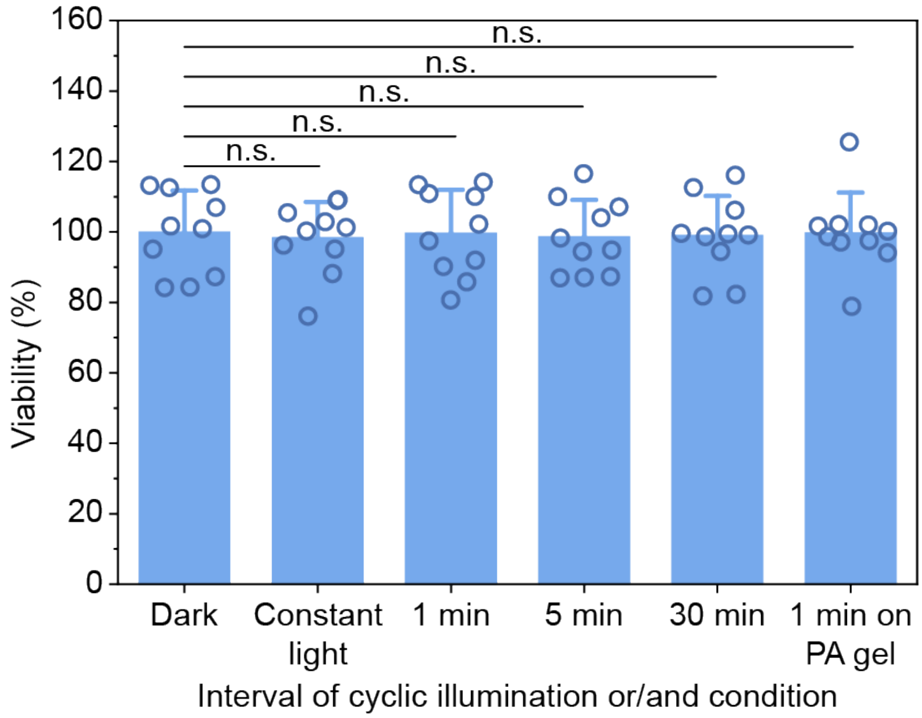

Figure S7 Viability of hMSCs seeded on PYP hydrogels under six different conditions for 48 h: (1) cultured on PYP hydrogels in dark; (2) cultured on PYP hydrogels under continuous blue light illumination; (3) cultured on PYP hydrogels upon cyclic illumination: 1 min on/off (transitioning between 2.2 kPa and 1.6 kPa); (4) cultured on PYP hydrogels upon cyclic illumination: 5 min on/off (transitioning between 2.2 kPa and 1.6 kPa); (5) cultured on PYP hydrogels upon cyclic illumination: 30 min on/off (transitioning between 2.2 kPa and 1.6 kPa); (6) cultured on PA hydrogels upon cyclic illumination: 1 min on/off (static Young's modulus of ~2.2 kPa). Cell Counting Kit-8 (1:10, KeyGen) was added to the culture medium. Then, the samples were analysed by a multimode microplate reader (Tecan, Infinite F50). Each from 10 independent experiments; n.s. represents $p > 0.1$, $p = 0.75$, 0.96, 0.79, 0.85, and 0.97 from left to right, unpaired, two-tailed t-test. Data are presented as mean values +/- standard deviation.

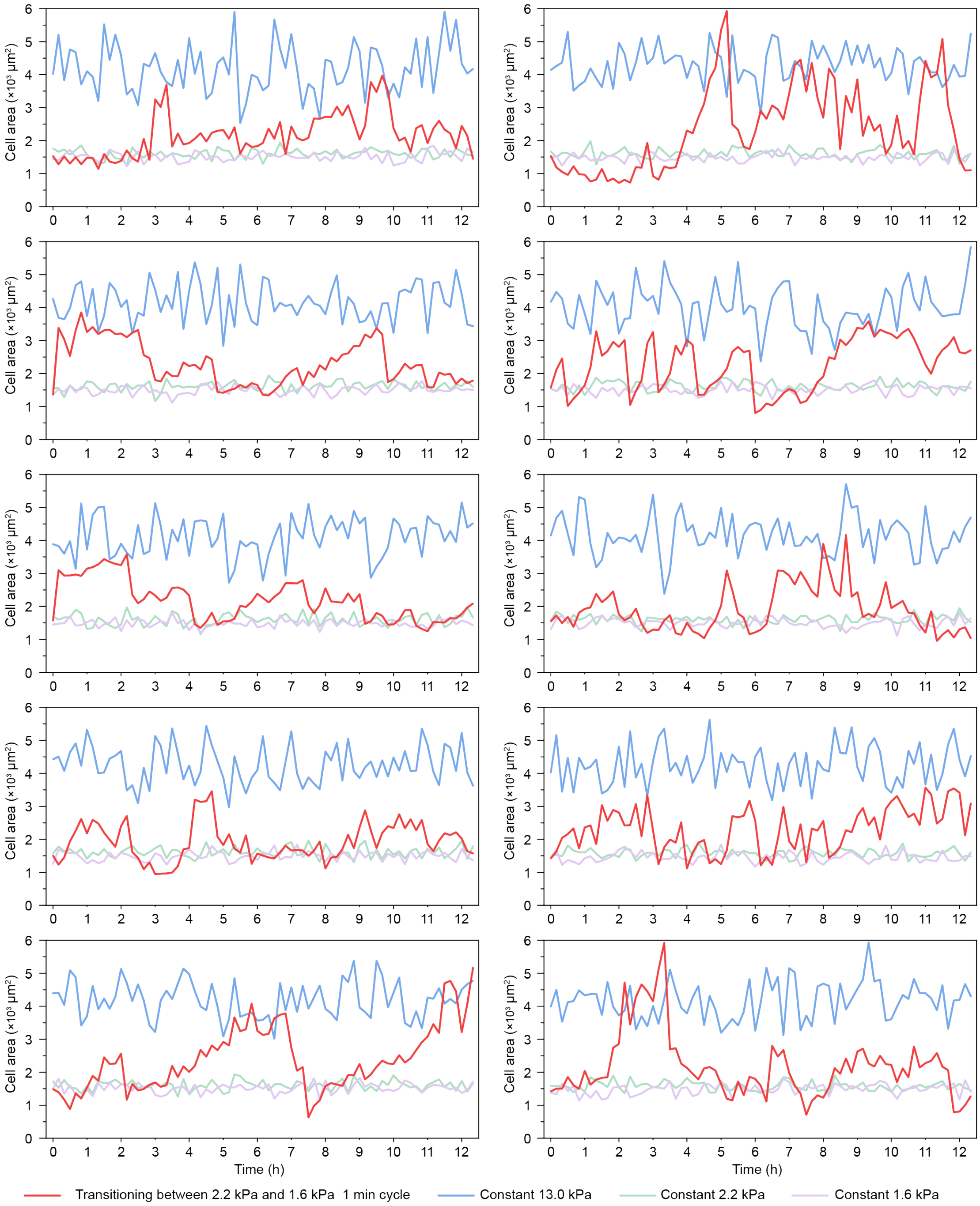

Figure S8 Cell area of individual hMSCs on the indicated PYP hydrogels prepared with different mechanical properties. Since the periodic changes in different cells do not occur at the same time, averaging these cell data would result in a flat line without significant fluctuations. Therefore, instead of averaging, extensive single-cell data were provided to better illustrate the morphological changes across individual cells.

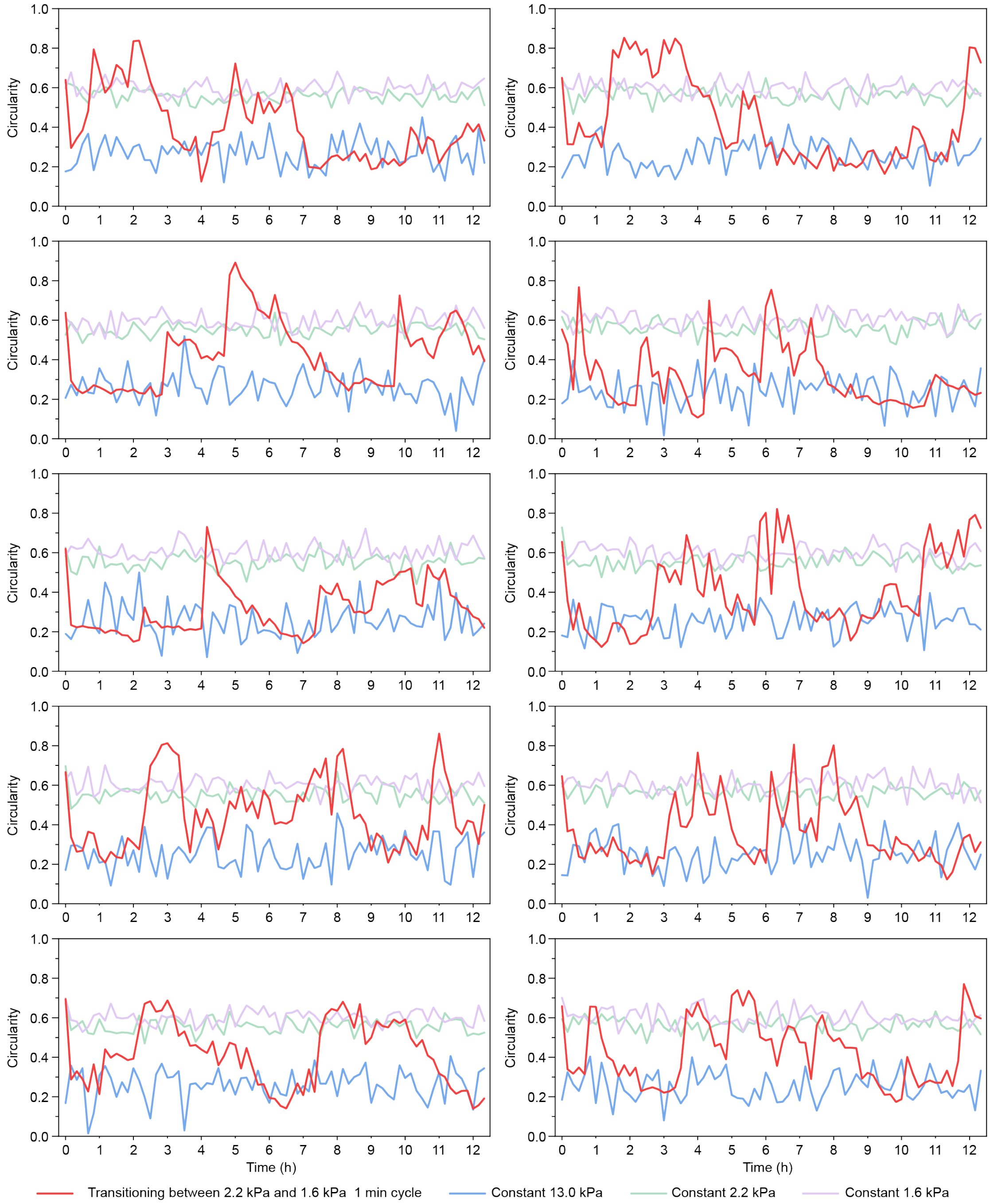

Figure S9 Circularity of individual hMSCs on the indicated PYP hydrogels prepared with different mechanical properties. Since the periodic changes in different cells do not occur at the same time, averaging these cell data would result in a flat line without significant fluctuations. Therefore, instead of averaging, extensive single-cell data were provided to better illustrate the morphological changes across individual cells.

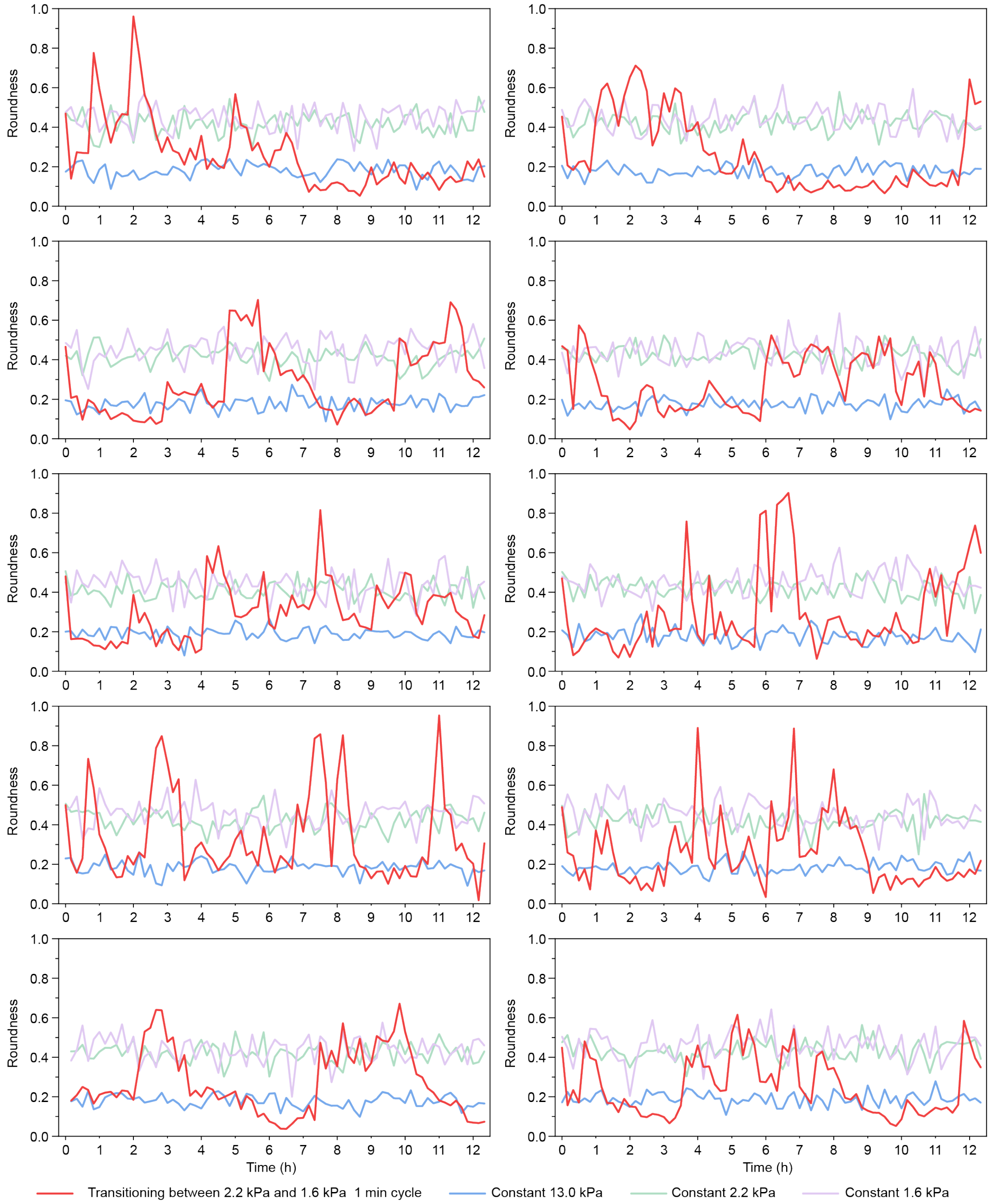

Figure S10 Roundness of individual hMSCs on the indicated PYP hydrogels prepared with different mechanical properties. Since the periodic changes in different cells do not occur at the same time, averaging these cell data would result in a flat line without significant fluctuations. Therefore, instead of averaging, extensive single-cell data were provided to better illustrate the morphological changes across individual cells.

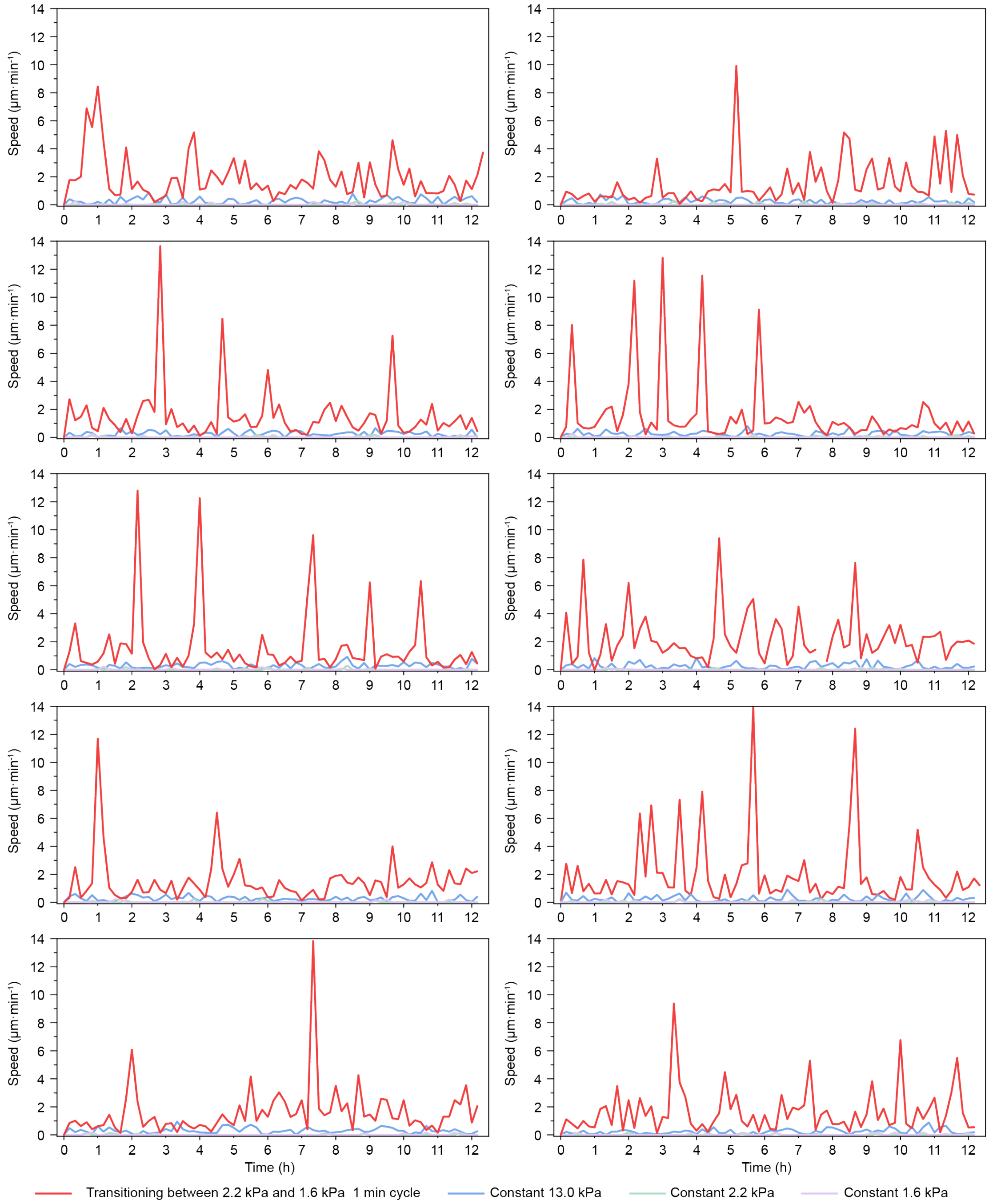

Figure S11 Instantaneous migration speed of individual hMSCs on the indicated PYP hydrogels prepared with different mechanical properties. Since the periodic changes in different cells do not occur at the same time, averaging these cell data would result in a flat line without significant fluctuations. Therefore, instead of averaging, extensive single-cell data were provided to better illustrate the morphological changes across individual cells.

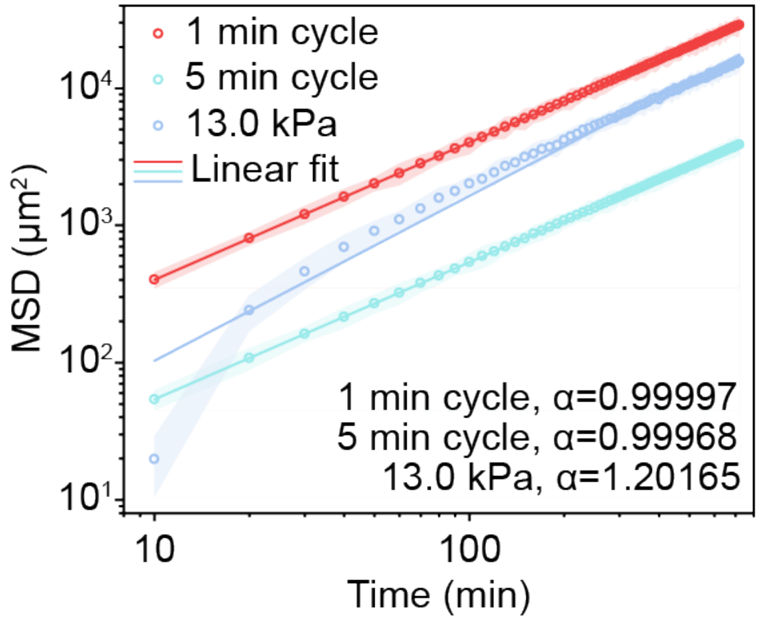

Figure S12 The log-log MSD plot of hMSCs on the indicated PYP hydrogels prepared with different mechanical properties. n=204, 202 and 219 (1 min cycle, 5 min cycle, and 13.0 kPa) cells were examined, each from 3 independent experiments. The experimental data are shown as the mean values (points) +/- standard deviation (shaded region).

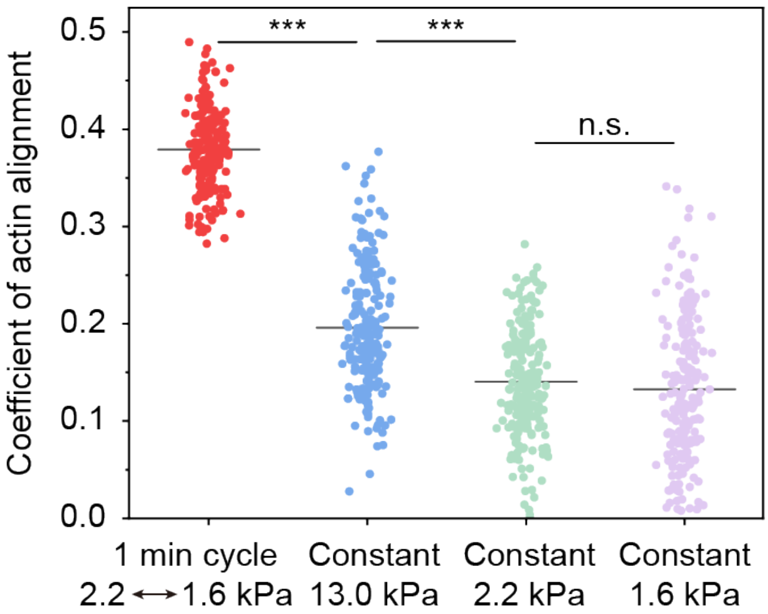

Figure S13 Coefficient of actin alignment of hMSCs on substrate with fast cyclic rigidity change and on static substrates (Young's modulus of ~13.0 kPa, 2.2 kPa, and 1.6 kPa). Coefficient of actin alignment under the 1-min cycles was significantly higher than that under static conditions. n=210, 203, 214 and 212 (2.2 kPa, 1.6 kPa, 13.0 kPa, and 1 min cycle) cells were examined, each from 3 independent experiments; *** represents $p < 0.01$, n.s. represents $p > 0.1$, p = 1.4E-118, 6.8E-20, and 0.23 from left to right, unpaired, two-tailed t-test.

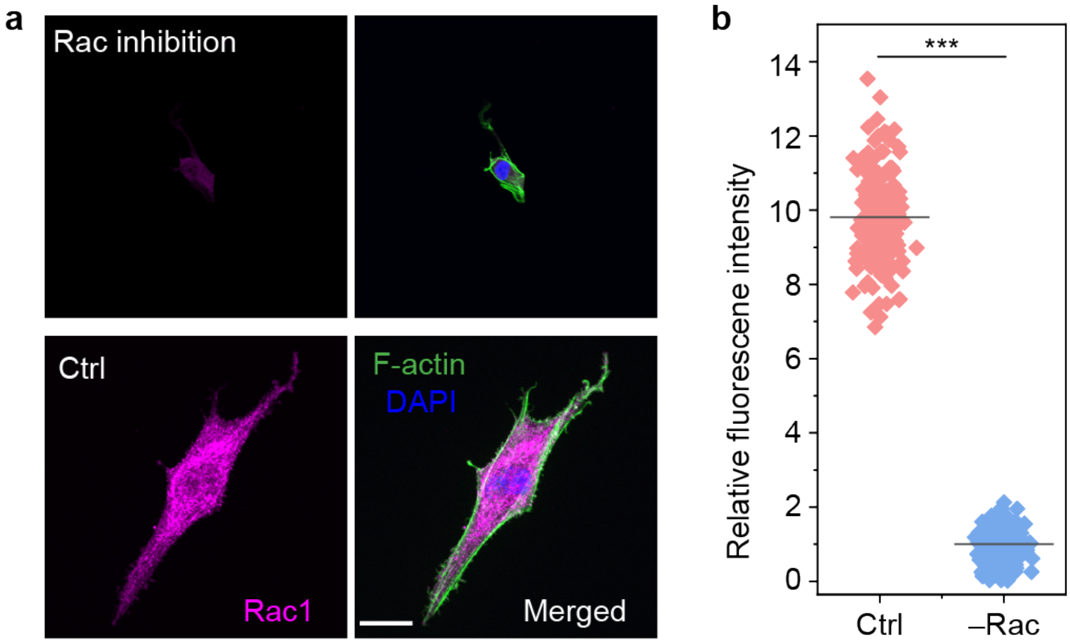

Figure S14 The effects of Rac1 inhibitors NSC23766 (–Rac) on the Rac1 level, as indicated by immunofluorescence. (a) Representative fluorescent images and (b) Statistics of the integrin level with and without Rac1 inhibitors NSC23766 (–Rac). The hMSCs were cultured for 12 h on glass with or without Rac1 inhibitors NSC23766 (10 μM) in the culture media. Scale bar is 50 μm. In b, n=197 and 198 (Ctrl and –Rac) cells were examined, each from 3 independent experiments; *** represents $p < 0.01$, $p = 7.1E\text{-}204$, unpaired, two-tailed t-test.

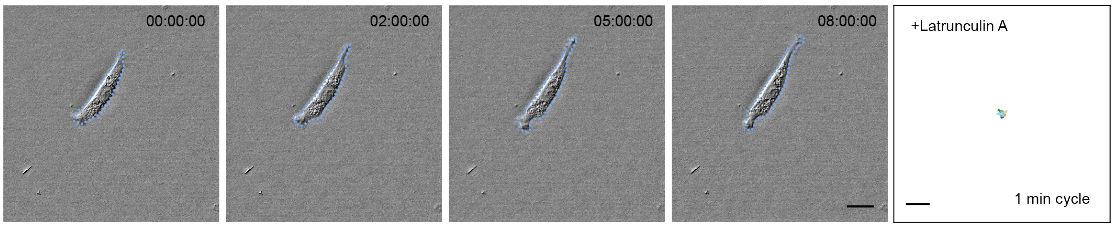

Figure S15 Time series of images of hMSC migration on PYP hydrogels with fast cyclic rigidity change with addition of latrunculin A (100 nM, +Lat. A). The far-right panel shows the trajectories of ~20 randomly selected migrating cells under the condition over 12 hours. Times are indicated in hour:minute:second. Scale bar is 50 μm for all panels.

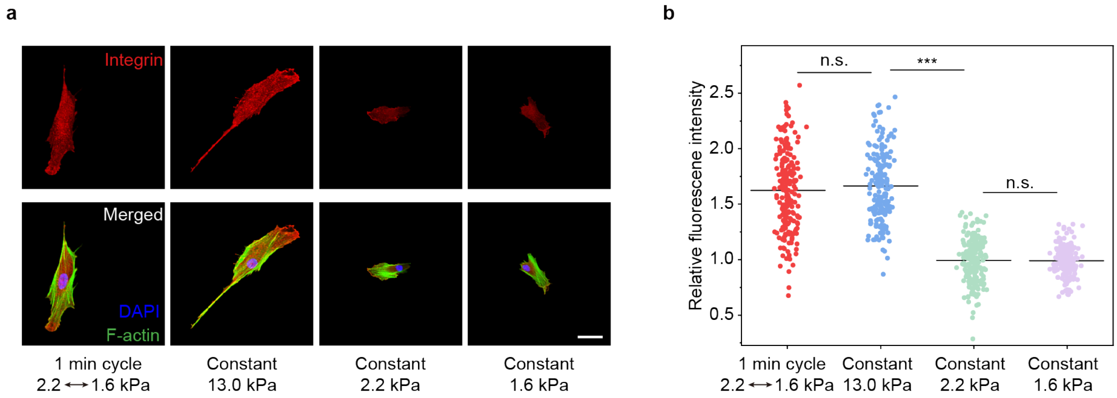

Figure S16 Recruitment of integrin of hMSCs on substrate with fast cyclic rigidity change and on static substrates (Young's modulus of ~13.0 kPa, 2.2 kPa, and 1.6 kPa), as indicated by immunofluorescence. (a) Representative fluorescent images and (b) Statistics of the integrin level under different conditions. Scale bar is 50 μm. In b, n=202, 201, 207 and 208 (2.2 kPa, 1.6 kPa, 13.0 kPa, and 1 min cycle) cells were examined, each from 3 independent experiments; *** represents $p < 0.01$, n.s. represents $p > 0.1$, $p = 0.12$, 4.5E-88, and 0.24 from left to right, unpaired, two-tailed t-test.

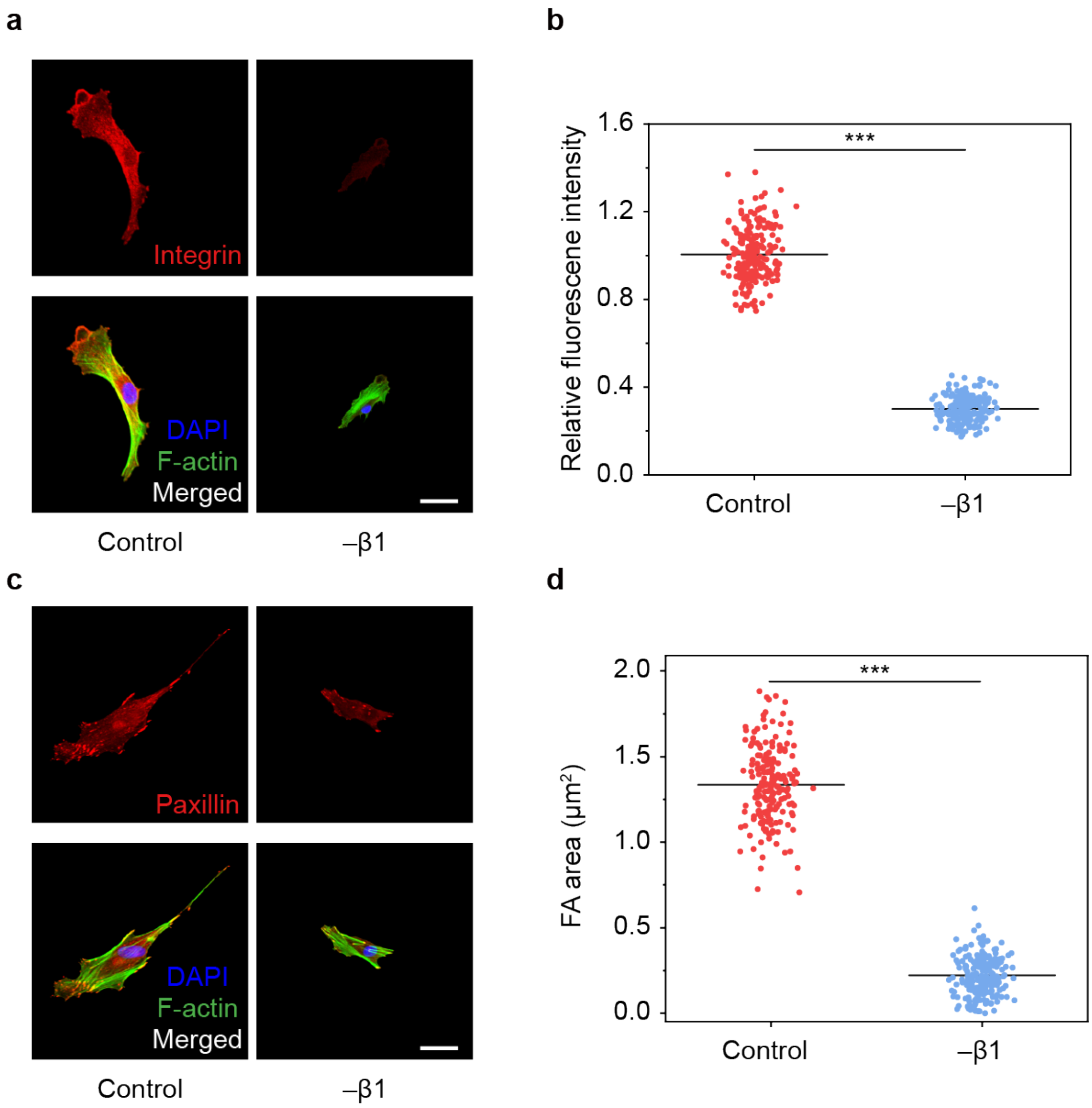

Figure S17 The effects of β1-integrin blocking (–β1) on the integrin level and the FA area, as indicated by immunofluorescence. (a) Representative fluorescent images and (b) Statistics of the integrin level with and without β1-integrin blocking. (c) Representative fluorescent images and (d) Statistics of the FA area with and without β1-integrin blocking on glass substrates. The hMSCs were cultured for 12 h on glass with or without β1-integrin blocking (5 μg ml^{-1}) in the culture media. Scale bar is 50 μm. In b, n=200 and 211 (Ctrl and –β1) cells were examined, each from 3 independent experiments, *** represents $p < 0.01$, p = 1.3E-182, unpaired, two-tailed t-test. In d, n=217 and 210 (Ctrl and –β1) cells were examined, each from 3 independent experiments, *** represents $p < 0.01$, p = 1.6E-195, unpaired, two-tailed t-test.

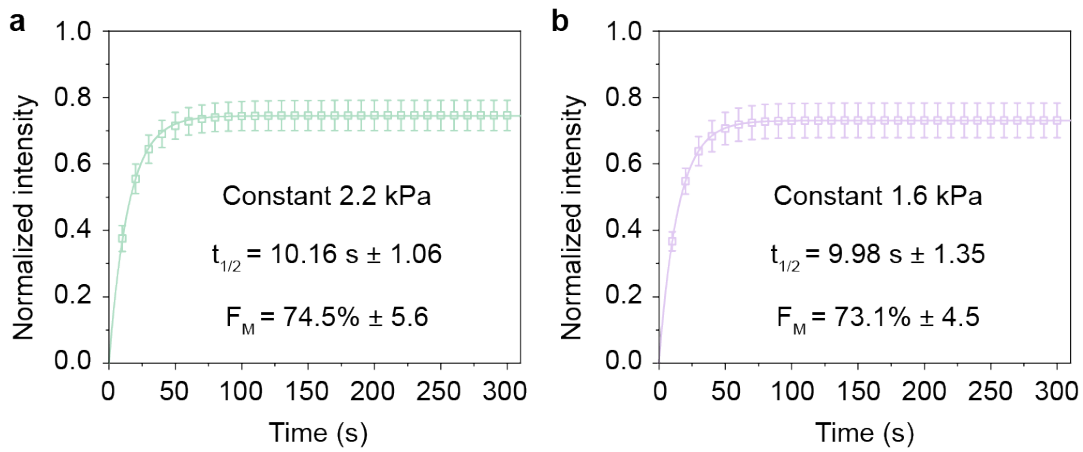

Figure S18 Focal adhesion dynamics of hMSCs on static substrates (Young's modulus of ~2.2 kPa, and 1.6 kPa), quantified through FRAP assays. In a-b, n= 193 and 191 (2.2 kPa and 1.6 kPa) cells were examined, each from 3 independent experiments. Data are presented as mean values +/- standard deviation.

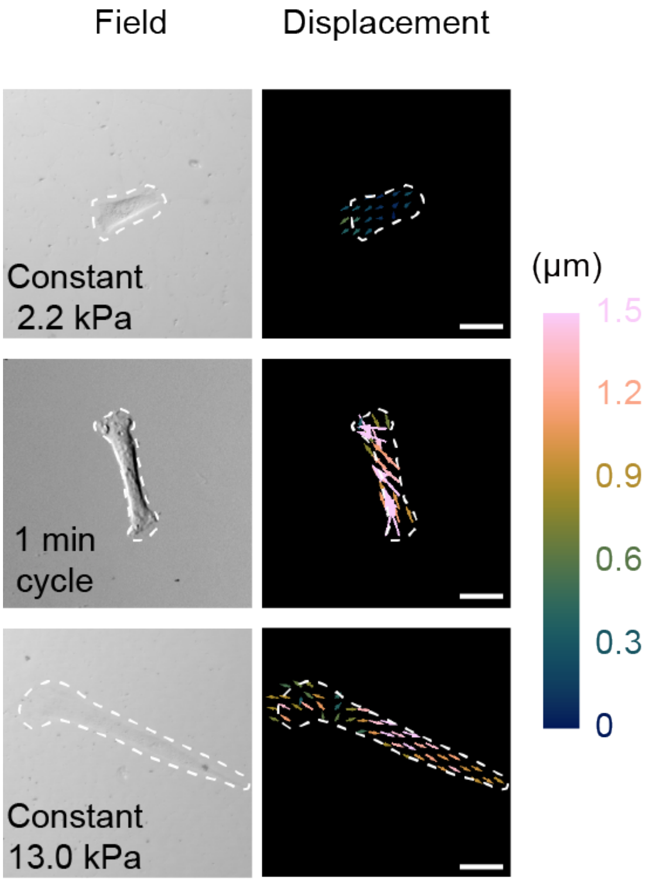

Figure S19 Deformation fields of hMSCs on static soft (Young's modulus of ~2.0 kPa) and rigid (Young's modulus of ~13.0 kPa) PYP hydrogels and on PYP hydrogel with rapid cyclic rigidity change (transitioning between 2.2 kPa and 1.6 kPa, 1 min on/off). Scale bar is 50 μm.

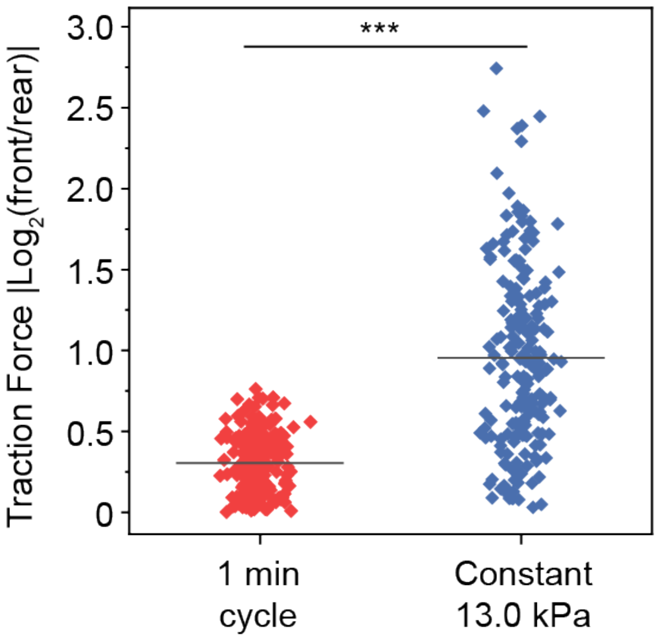

Figure S20 Quantification of cell adhesion forces polarity on the two sides from hMSCs on the indicated PYP hydrogels with fast cyclic rigidity change and on static rigid substrates (Young's modulus of ~13.0 kPa). n= 193 and 196 (1 min cycle and 13.0 kPa) cells were examined, each from 3 independent experiments, *** represents $p < 0.01$, $p = 1.3E-37$, unpaired, two-tailed t-test.

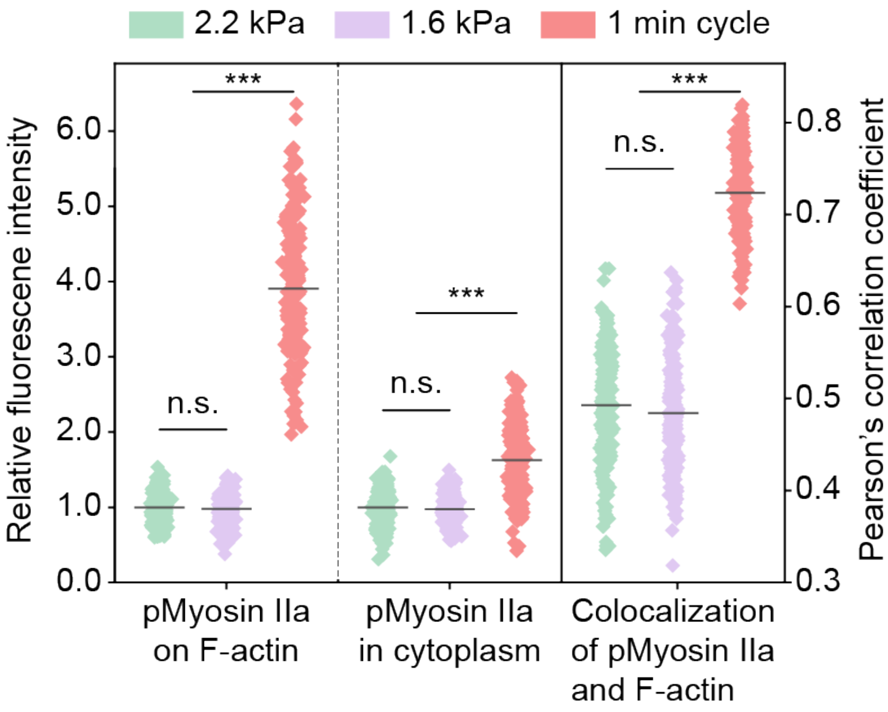

Figure S21 The pMyosin IIa level on F-actin and in cytoplasm on the indicated PYP hydrogels prepared with different mechanical properties, along with Pearson's correlation coefficient analysis of pMyosin IIa and F-actin colocalization, as assessed by immunofluorescence imaging. n=213, 219 and 205 (2.2 kPa, 1.6 kPa, and 1 min cycle) cells were examined, each from 3 independent experiments; *** represents $p < 0.01$, n.s. represents $p > 0.1$, p = 0.17, 9.8E-119, 0.14, 1.8E-48, 0.11 and 2.9E-156 from left to right, unpaired, two-tailed t-test.

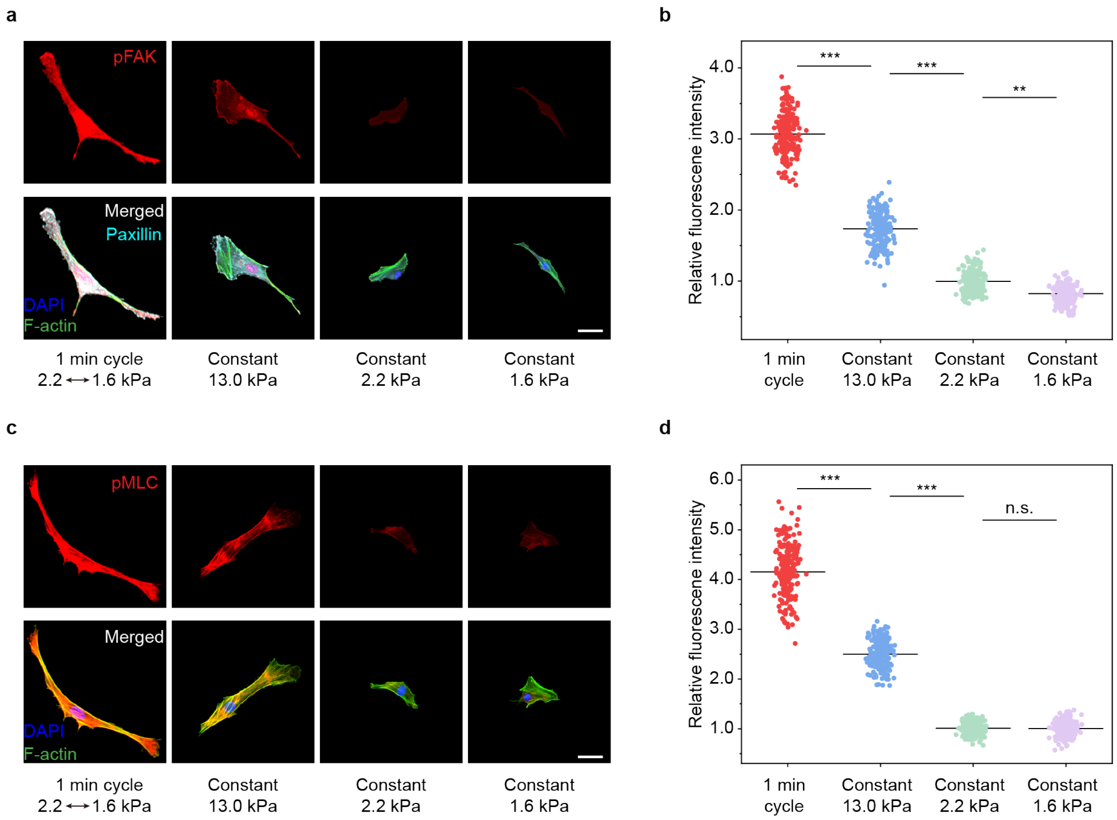

Figure S22 Mechnosignalling protein pFAK and pMLC level of hMSCs on substrate with fast cyclic rigidity change (transitioning between 2.2 kPa and 1.6 kPa, 1 min on/off) and on static substrates (Young's modulus of ~13.0 kPa, 2.2 kPa, and 1.6 kPa), as indicated by immunofluorescence. (a) Representative fluorescent images and (b) Statistics of mechnosignalling protein pFAK. (c) Representative fluorescent images and (d) Statistics of mechnosignalling protein pMLC. Scale bar is 50 μm. In b, n=207, 203, 218 and 222 (2.2 kPa, 1.6 kPa, 13.0 kPa, and 1 min cycle) cells were examined, each from 3 independent experiments; *** represents $p < 0.01$, ** represents $p < 0.1$, p = 1.1E-189, 4.4E-138 and 0.011 from left to right, unpaired, two-tailed t-test. In d, n=219, 217, 211 and 225 (2.2 kPa, 1.6 kPa, 13.0 kPa, and 1 min cycle) cells were examined, each from 3 independent experiments; *** represents $p < 0.01$, n.s. represents $p > 0.1$, p = 6.6E-136, 1.2E-189 and 0.73 from left to right, unpaired, two-tailed t-test.

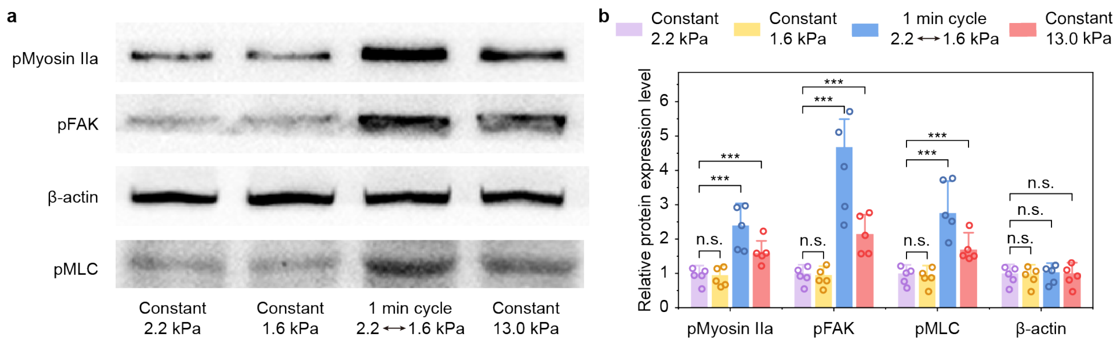

Figure S23 The phosphorylation levels of Myosin IIa, FAK, and MLC of hMSCs on substrate with fast cyclic rigidity change (transitioning between 2.2 kPa and 1.6 kPa, 1 min on/off) and on static substrates (Young's modulus of ~13.0 kPa, 2.2 kPa, and 1.6 kPa), as indicated by Western blotting. The phosphorylation level under the 1-min cycles was significantly higher than that under static conditions (Young's modulus of ~13.0 kPa, 2.2 kPa, and 1.6 kPa). In b, data are presented as mean values +/- standard deviation, each from 5 independent experiments; *** represents $p < 0.01$, n.s. represents $p > 0.1$, $p = 0.76$, 0.0058, 0.0093, 0.77, 0.0067, 0.0078, 0.77, 0.0038, 0.0078, 0.90, 0.84 and 0.98 from left to right, unpaired, two-tailed t-test.

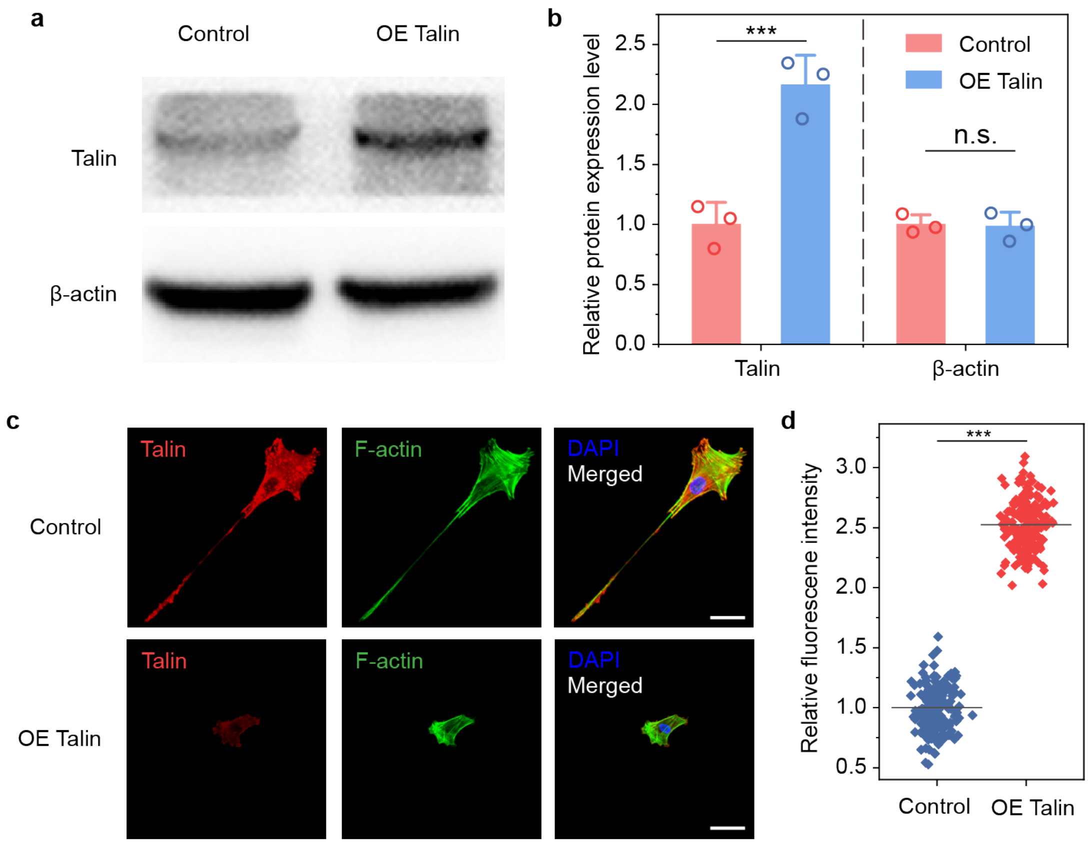

Figure S24 The effects of transfecting hMSCs with the OE Talin plasmid on Talin level, as indicated by Western blotting and immunofluorescence. (a) Representative Western blots and (b) Statistics of Talin; In b, data are presented as mean values +/- standard deviation, each from 3 independent experiments; *** represents $p < 0.01$, n.s. represents $p > 0.1$, $p = 0.0037$ and 0.86 from left to right, unpaired, two-tailed t-test. (c) Representative fluorescent images and (d) Statistics of Talin. The results show that Talin is overexpressed in hMSCs transfected with the OE Talin plasmid. Scale bar is 50 μm. In d, n=181 and 183 (Ctrl and OE Talin) cells were examined, each from 3 independent experiments, *** represents $p < 0.01$, $p = 2.0E-222$, unpaired, two-tailed t-test.

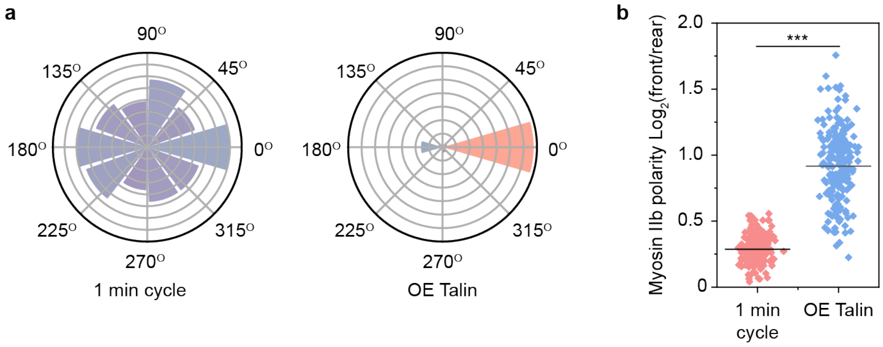

Figure S25 Quantitative analysis of hMSC migration on soft PYP hydrogels with rapid cyclic rigidity changes, comparing conditions with Talin overexpression (OE Talin) and without (1 min cycle). (a) Quantitative analysis of cell migration directions. (b) Quantitative analysis of Myosin IIb intensity polarity across the two sides of hMSCs. n=202 and 205 (1 min cycle and OE Talin) cells were examined, each from 3 independent experiments, *** represents $p < 0.01$, $p = 1.7E-93$, unpaired, two-tailed t-test.

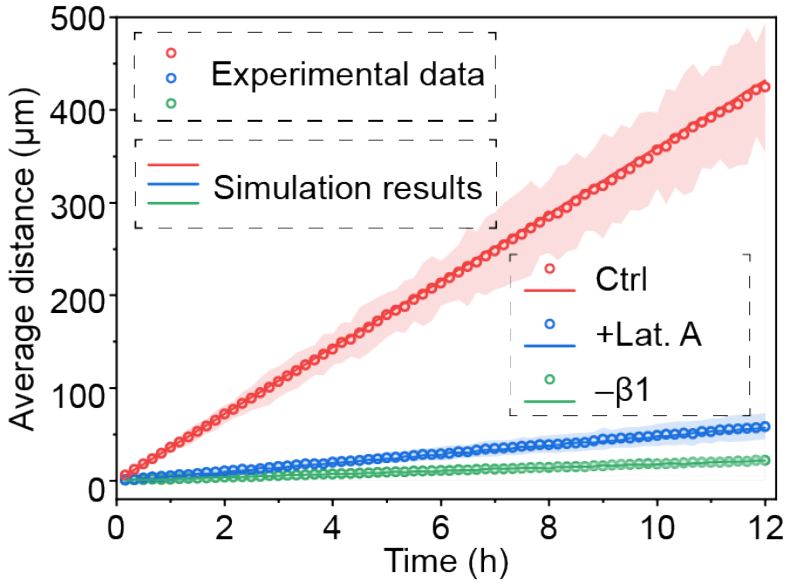

Figure S26 Average migration distance of hMSCs on substrates with fast cyclic rigidity changes, halving the actin polymerization rate (+Lat. A) and reducing the number of clutches (–β1) in the experiments and simulations. n=204, 186 and 181 (Ctrl, +Lat. A, and –β1) cells were examined, each from 3 independent experiments. The experimental data are presented as the mean values (points) +/- standard deviation (shaded region); the simulation results are shown as the mean values (solid line).

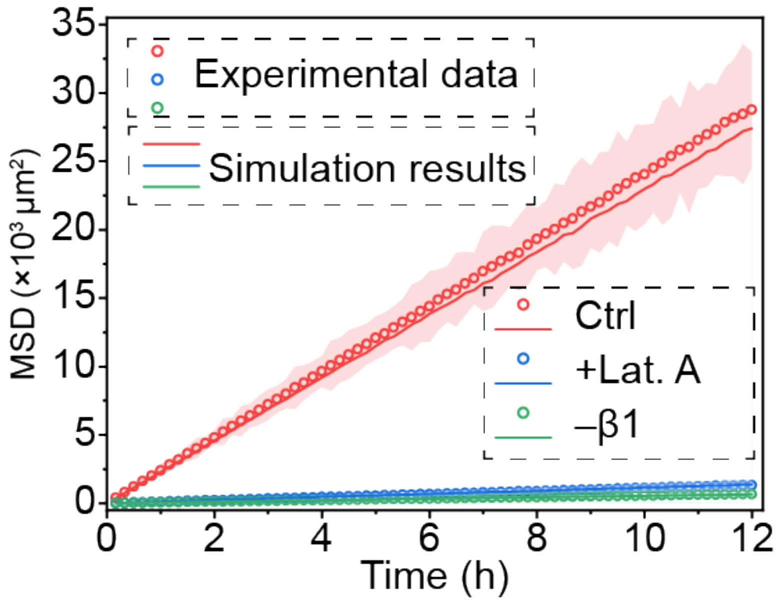

Figure S27 Mean square displacement (MSD) of hMSCs on substrates with fast cyclic rigidity changes, halving the actin polymerization rate (+Lat. A) and reducing the number of clutches (–β1) in the experiments and simulations. n=204, 177 and 176 (Ctrl, +Lat. A, and –β1) cells were examined, each from 3 independent experiments. The experimental data are presented as the mean values (points) +/- standard deviation (shaded region); the simulation results are shown as the mean values (solid line).

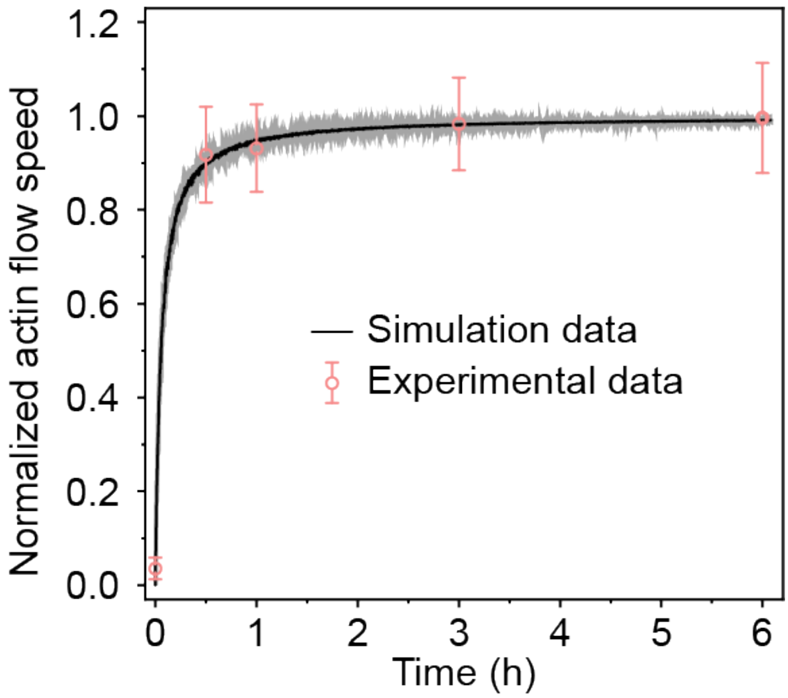

Figure S28 Actin flow speed of hMSCs on substrates with fast cyclic rigidity changes (1 min cycle) in the experiments and simulations. n=180, 214, 206, 190 and 179 (0 h, 0.5 h, 1 h, 3 h, and 6 h) cells were examined, each from 3 independent experiments. The simulation results are shown as the mean values (solid line) +/- standard deviation (shaded region), which reflects the predicted variability. The experimental data are presented as the mean values (points) +/- standard deviation (error bars).

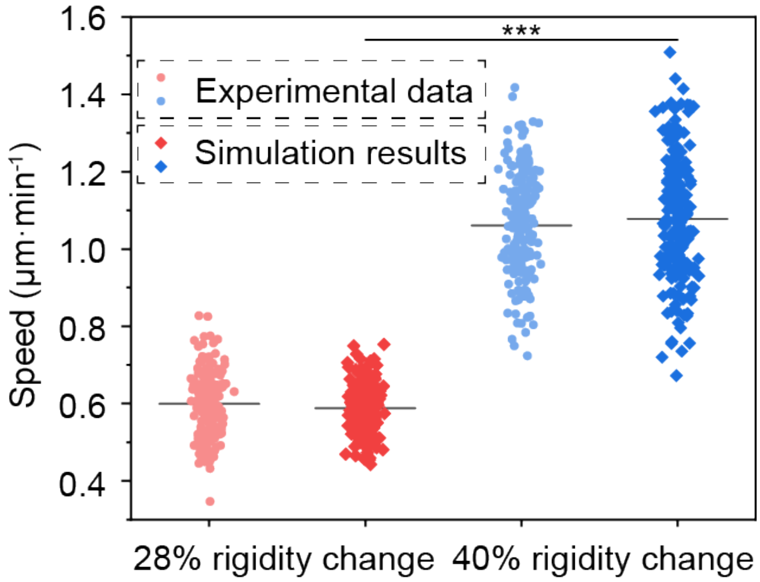

Figure S29 Average migration speed of hMSCs on substrates with fast cyclic rigidity changes with different softening amplitude from the rigid state (28% and 40% of the rigid state) predicted by our simulation and validated by experiments. n=204 and 213 (28% and 40%) cells were examined, each from 3 independent experiments, *** represents $p < 0.01$, $p = 1.8E\text{-}116$, unpaired, two-tailed t-test.

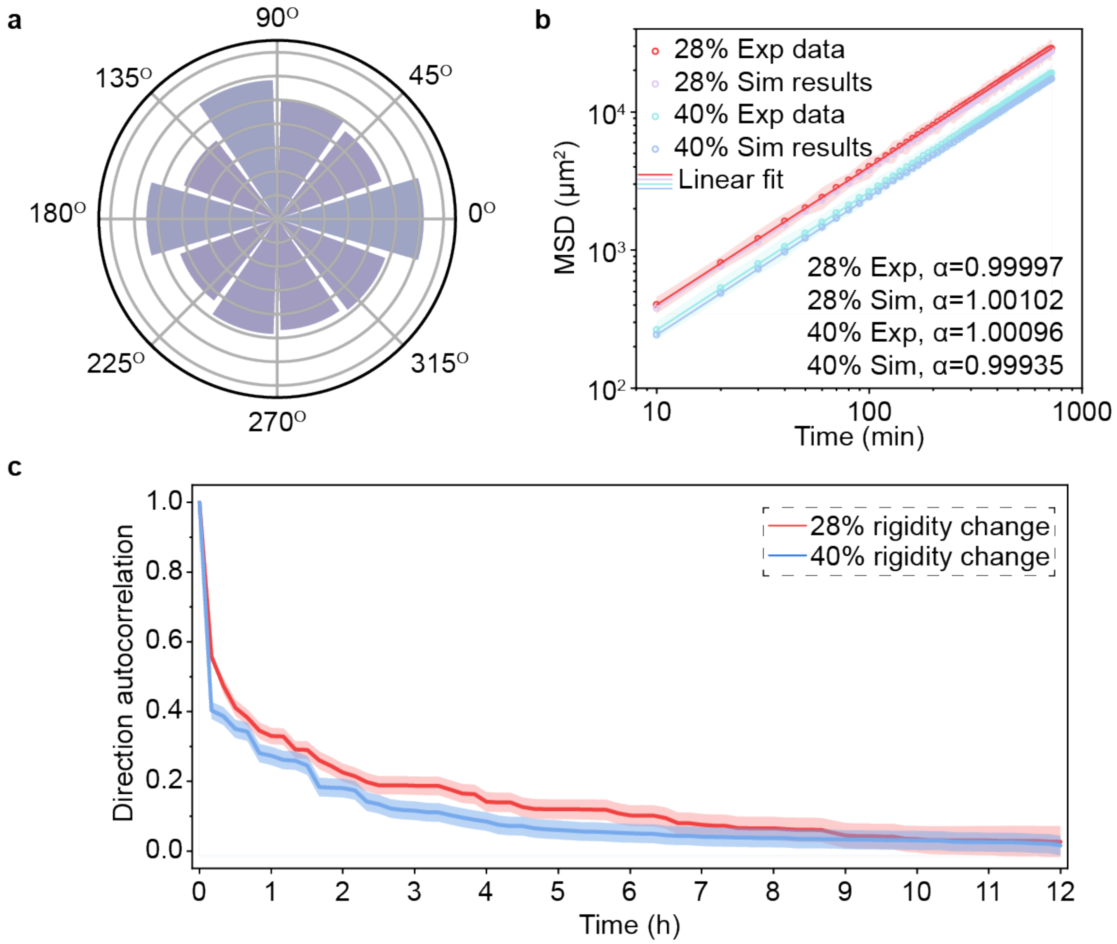

Figure S30 (a) Quantitative analysis of directions of cell migration on substrate with fast cyclic rigidity change with 40% softening amplitude from the rigid state (transitioning between 2.2 kPa and 1.3 kPa, 1 min on/off). (b) The log-log MSD plot of hMSCs on substrates with fast cyclic rigidity changes with different softening amplitude from the rigid state (28% and 40% of the rigid state) predicted by our simulation and validated by experiments. The experimental data are presented as mean values (points) +/- standard deviation (shaded region). (c) Quantitative analysis of direction autocorrelation of cell migration on substrate with fast cyclic rigidity change with different softening amplitude from the rigid state (28% and 40% of the rigid state). Data are presented as mean values (central line) +/- standard deviation (shaded region). In all panels, n= 204 and 213 (28% and 40%) cells were examined, each from 3 independent experiments.

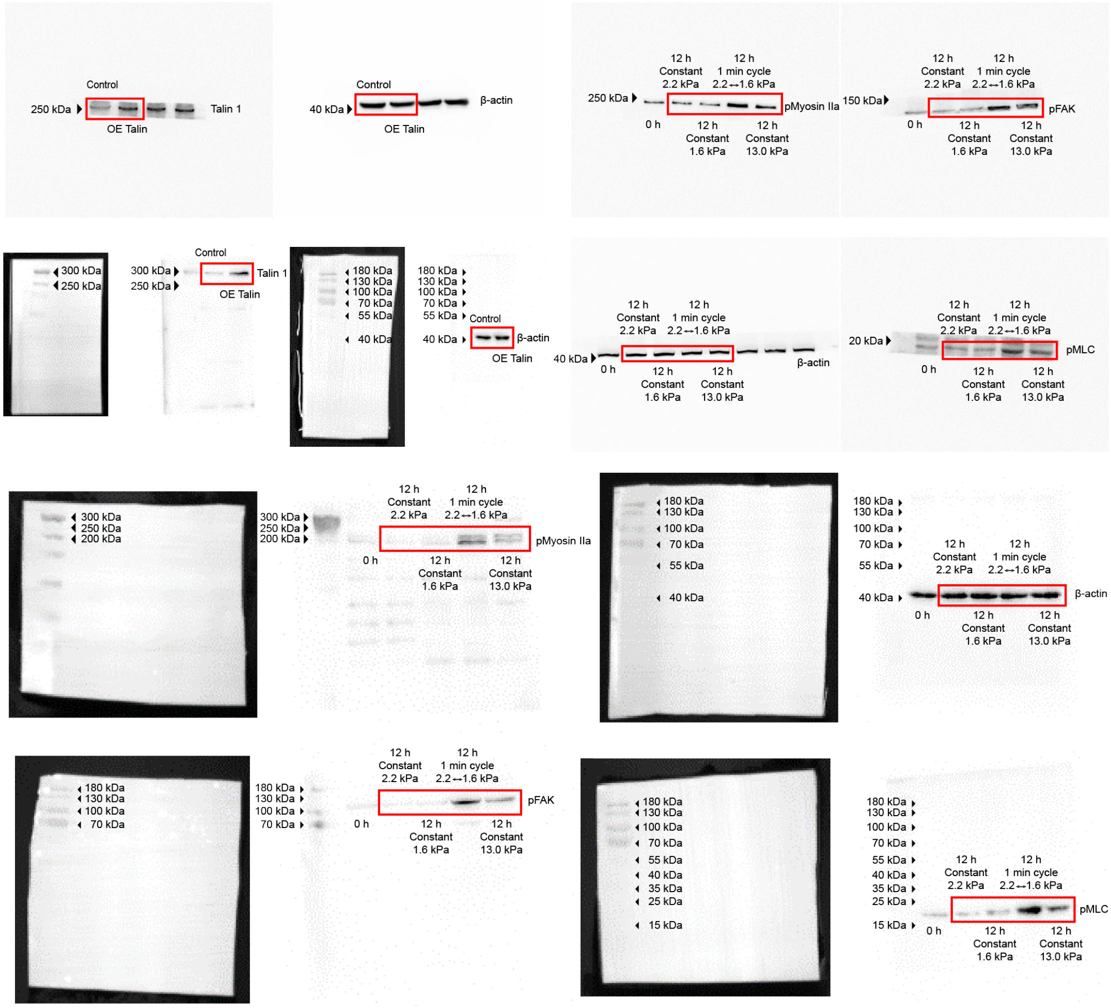

Figure S31 Uncropped blots.

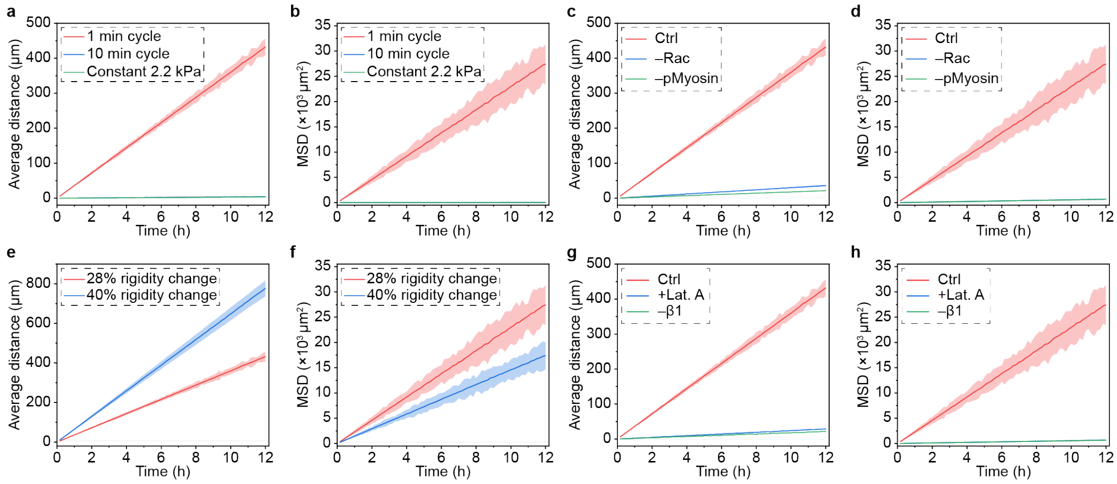

Figure S32 Simulation results with associated predictive variability.

(a-b) Average migration distance and MSD of hMSCs on substrates prepared with different mechanical properties over 12 h, predicted by our simulation. (c-d) Average migration distance and MSD of hMSCs on substrates with fast cyclic rigidity changes over 12 h, slowing the actin polymerization rate (–Rac) and lowering the number of motors (–pMyosin), predicted by our simulation. (e-f) Cell elongation, average migration distance and MSD of hMSCs on substrates with fast cyclic rigidity changes with different softening amplitude from the rigid state (28% and 40% of the rigid state), predicted by our simulation. (g-i) Average migration distance and MSD of hMSCs on substrates with fast cyclic rigidity changes, halving the actin polymerization rate (+Lat. A) and reducing the number of clutches (–β1), predicted by our simulation. In all panels, the simulation results are presented as mean values (central line) +/- standard deviation (shaded region), calculated from 200 independent simulation runs.

Reference

1 Chan, C. E. & Odde, D. J. Traction Dynamics of Filopodia on Compliant Substrates. *Science* **322**, 1687-1691 (2008). https://doi.org/doi:10.1126/science.1163595

2 Gong, Z. *et al.* Matching material and cellular timescales maximizes cell spreading on viscoelastic substrates. *Proc Natl Acad Sci U S A* **115**, E2686-e2695 (2018). https://doi.org/10.1073/pnas.1716620115

3 Cheng, B. *et al.* Nanoscale integrin cluster dynamics controls cellular mechanosensing via FAKY397 phosphorylation. *Sci Adv* **6**, eaax1909 (2020). https://doi.org/10.1126/sciadv.aax1909